HHS Public Access

Author manuscript

Ann Eye Sci. Author manuscript; available in PMC 2021 March 30.

Published in final edited form as:

Ann Eye Sci. 2021 March ; 6: . doi:10.21037/aes-20-12.

Hyperspectral autofluorescence characterization of drusen and sub-RPE deposits in age-related macular degeneration

Yuehong Tong[1], **Thomas Ach**[2], **Christine A. Curcio**[3], **R. Theodore Smith**[1]

[1]Department of Ophthalmology, Icahn School of Medicine at Mount Sinai, New York, NY, USA;

[2]Department of Ophthalmology, University Hospital Bonn, Germany;

[3]Department of Ophthalmology and Visual Sciences, University of Alabama at Birmingham, AL, USA

Abstract

Background: Soft drusen and basal linear deposit (BLinD) are two forms of the same extracellular lipid rich material that together make up an Oil Spill on Bruch's membrane (BrM). Drusen are focal and can be recognized clinically. In contrast BLinD is thin and diffusely distributed, and invisible clinically, even on highest resolution OCT, but has been detected on *en face* hyperspectral autofluorescence (AF) imaging *ex vivo*. We sought to optimize histologic hyperspectral AF imaging and image analysis for recognition of drusen and sub-RPE deposits (including BLinD and basal laminar deposit), for potential clinical application.

Methods: Twenty locations specifically with drusen and 12 additional locations specifically from fovea, perifovea and mid-periphery from RPE/BrM flatmounts from 4 AMD donors underwent hyperspectral AF imaging with 4 excitation wavelengths (λ_{ex} 436, 450, 480 and 505 nm), and the resulting image cubes were simultaneously decomposed with our published non-negative matrix

Correspondence to: R. Theodore Smith, Department of Ophthalmology, Icahn School of Medicine at Mount Sinai, 1468 Madison Avenue, Annenberg 22-86, Box 1183, New York, NY 10029-6574, USA. rts1md@gmail.com.

Contributions: (I) Conception and design: All authors; (II) Administrative Support: Y Tong, RT Smith; (III) Provision of study materials or patients: T Ach, CA Curcio; (IV) Collection and assembly of data: Y Tong, RT Smith; (V) Data analysis and interpretation: All authors; (VI) Manuscript writing: All authors; (VII) Final approval of manuscript: All authors.

Reporting Checklist: The authors have completed the MDAR reporting checklist. Available at http://dx.doi.org/10.21037/aes-20-12

Data Sharing Statement: Available at http://dx.doi.org/10.21037/aes-20-12

Ethical Statement: The authors are accountable for all aspects of the work in ensuring that questions related to the accuracy or integrity of any part of the work are appropriately investigated and resolved. These are not human subject experiments, so IRB and Helsinki declaration are not required.

Conflicts of Interest: The authors have completed the ICMJE uniform disclosure form (available at http://dx.doi.org/10.21037/aes-2020-rid-08). The series "Retinal Imaging and Diagnostics" was commissioned by the editorial office without any funding or sponsorship. Dr. Smith served as the unpaid Guest Editor of the series, and serves as an unpaid editorial board member of *Annals of Eye Science* from May 2019 to Apr 2021. Dr. Ach reports grants from NIH/NEI 1R01EY027948, during the conduct of the study; other from Macregen, outside the submitted work. Dr. Curcio reports other from MacRegen, outside the submitted work; and Research support from Heidelberg Engineering and Genentech/ Hoffman LaRoche. Dr. Smith reports other from MacRegen, outside the submitted work; In addition, Dr. Smith has a patent the multi excitation image analysis technique for hyperspectral AF imaging issued. The authors have no other conflicts of interest to declare.

factorization (NMF). Rank 4 recovery of 4 emission spectra was chosen for each excitation wavelength.

Results: A composite emission spectrum, sensitive and specific for drusen and presumed sub-RPE deposits (the SDr spectrum) was recovered with peak at 510–520 nm in all tissues with drusen, with greatest amplitudes at excitations λ_{ex} 436, 450 and 480 nm. The RPE spectra of combined sources Lipofuscin (LF)/Melanolipofuscin (MLF) were of comparable amplitude and consistently recapitulated the spectra S1, S2 and S3 previously reported from all tissues: tissues with drusen, foveal and extra-foveal locations.

Conclusions: A clinical hyperspectral AF camera, with properly chosen excitation wavelengths in the blue range and a hyperspectral AF detector, should be capable of detecting and quantifying drusen and sub-RPE deposits, the earliest known lesions of AMD, before any other currently available imaging modality.

Keywords

Age-related macular degeneration; sub-RPE deposits; drusen; hyperspectral autofluorescence (AF)

Introduction

Age-related macular degeneration (AMD) is the leading cause of vision loss in adults over 60 in the developed world. Drusen are a hallmark for AMD (1–4). Large soft drusen as well as basal linear deposits (BLinD) (5), which are soft drusen material spread in a thin diffuse layer, are the lipid rich materials of the Oil Spill on Bruch's membrane (BrM) that is specific for early/intermediate AMD (6). Both increase the risk of progression to advanced AMD, but only drusen can be detected on clinical exam. BLinD and drusen, along with basal laminar deposit (BLamD), constitute a diffusion barrier for the supply of the outer retina with oxygen and nutrients from the choroid, the offloading of unneeded metabolites, and a stimulus to neovascularization. Hence these deposits are implicated in AMD pathology and might be important therapeutic targets. Drusen are focal and recognizable clinically using color fundus photography (7), optical coherence tomography (OCT) (8) and advanced spectral domain (SD)-OCT (9). BLinD is thin, diffuse, and invisible clinically, even on high resolution OCT. BLamD may be visible if very thick (10).

On the other hand, spectrally resolved autofluorescence (AF) imaging of RPE/BrM flatmounts *ex vivo* reveals distinct spectra S1, S2 and S3 of RPE (LF/MLF), S0 of Bruch's membrane (BrM), and SDr of drusen and sub-RPE deposits (11,12). Sub-RPE deposits is a collective term for BLinD and BLamD, which could be definitively separated by transmission electron microscopy or high-resolution light microscopy (13). This suggests that the AF spectra of drusen and sub-RPE deposits may be detectable clinically with suitable hyperspectral AF imaging, despite the fact that anatomically thin BLinD is not detectable by IR reflectance on SD-OCT and BLamD is visible only when thick. This in turn would offer a new method to help diagnose AMD at an early stage.

Drusen are classified as small (<63 μm diameter); intermediate (63–124 μm); and large (≥125 μm). In a recent clinical classification (7), AMD itself is classified as early, with only

small/intermediate drusen and no retinal pigmentary changes; intermediate, with large soft drusen or multiple intermediate drusen with pigment abnormalities (7); and late, with neovascular or atrophic changes (7). Drusen are also classified into hard and soft on their imaging appearance.

Hyperspectral imaging is a general imaging modality combining spectral and spatial data. Hyperspectral images are acquired from the same 2D scene at multiple narrow spectral bands. The resulting stack of images is called a hyperspectral cube that contains two spatial dimensions and one spectral dimension. By decomposing hyperspectral data, one can identify the main spectral signatures and their corresponding abundance images (11,12). It is employed in multiple diverse scenarios such as the assessment of food quality and safety (14,15), trace detection in forensic science (16), and cellular processes in medical science (17–19). In the clinic, It is used to detect cancer (20–23), assess diabetic foot disease (24,25), detect arthritis (26), monitor oxygen saturation in the retinal vessels (27), and deliver real-time tissue characterization for surgical guidance (28,29). Because hyperspectral imaging is non- invasive, it is an ideal method for clinical use.

We previously visualized soft drusen and related sub-RPE deposits in flat mounts of human donor eyes (*ex vivo*) using hyperspectral AF images (11) at excitation wavelengths λ_{ex} 436 and 480 nm. In this study we additionally introduce λ_{ex} 450 and 505 nm to optimize the excitation wavelengths for a proposed clinical hyperspectral AF camera. Indeed, we found that the emission spectral signatures of drusen and sub-RPE deposits at λ_{ex} 436 and 450 nm wavelengths were essentially identical in shape, and comparable in amplitude. These results support the incorporation of λ_{ex} 450 nm in a clinical hyperspectral AF camera for the early detection of AMD deposits. We present the following article in accordance with the MDAR reporting checklist (available at http://dx.doi.org/10.21037/aes-20-12).

Methods

RPE/BrM flat mounts were prepared from retina tissues from 4 white donors with AMD, as previously described (30). Age and sex were 81M, 83F, 85M, and 88F. We selected 5 locations with drusen from each donor tissue for imaging with an upright microscope equipped with a 40x oil-immersion objective (numerical aperture = 1.4; Axio Imager A2, Carl Zeiss, Jena, Germany). Drusen dimensions were measured on the 40×, 1,390×1,038 dimension images in Photoshop (50 microns = 200 pixel). An external mercury arc light source (X-Cite 120Q, Lumen Dynamics Group, Inc., Mississauga, Ontario, Canada) provided excitation light through dichroic filter cubes (centers of band pass excitations/long pass emissions = 436/460 nm, 450/495 nm, 480/510 nm and 505/520 nm; Chroma Technology Corp., Bellows Falls, VT, USA). Excitation wavelengths were thus centered at λ_{ex} 436, 450, 480 and 505 nm. Hyperspectral emission image stacks with these 4 excitations were captured from 420 to 720 nm in 10 nm increments by a hyperspectral Camera (Nuance FX, Caliper LifeSciences, Waltham, MA, USA).

As a secondary goal, we also imaged 3 specific anatomic locations from each donor: fovea, perifovea and mid-periphery, in addition to the drusen locations. The purpose was to determine if the recovered LF/MLF spectra differed at these locations, in light of new

findings about the actual tissue distribution of LF and MLF granules (31) that show MLF are much more abundant than LF in the fovea, and the reverse elsewhere.

We analyzed the data using customized software and non-negative matrix factorization (NMF) as previously described (11,32). A 3-Gaussian initialization was fit to the LF spectrum (corrected for BrM) and a fourth channel was directly read from BrM in the tissue. We therefore obtained up to four independent recovered spectra and their corresponding abundance images that exhibited the spatial localization of each recovered signal. In some cases, only 3 independent spectra were recovered, as will be discussed.

Statistical analysis

Means and standard deviation (SD) were the statistical metrics calculated for the interpretation of the spectral data in this study. The spectral peaks in each group of spectra were expressed as mean ± SD.

Results

For drusen locations—There were a total of 34 drusen: 17 small; 16 intermediate; and 1 large. We extracted specific spectra for the drusen and sub-RPE deposits from all samples when the tissues were excited at λ_{ex} 436 and 450 nm. These spectra were nearly identical, with peaks within 10 nm of 520 nm, in each of the 20 tissue locations, and replicated the spectral signature SDr at 436 nm excitation in our previous report (11). The ubiquitous spectrum S0 (mean peak 495 at excitation 436 nm). We previously reported from BrM in normal RPE/BrM flat mounts (11) was not observed in any tissue, but was replaced by SDr as the shortest wavelength spectrum recovered. The emission spectrum from drusen and sub-RPE deposits (SDr) from λ_{ex} 436 and 450 nm excitation peaked at mean 512±6.5 nm and 516±6.1 nm, respectively. No differences were detected in SDr recovered from drusen of different sizes. Abundance images for SDr localized to drusen and apparent sub-RPE deposits in all cases. Previously reported RPE spectra S1 and S2 were observed in all drusen locations; S3 appeared only in samples from one donor (88F). At 436 nm excitation, the spectra S1, S2 and S3 peaked at 539±14.1 nm, 576±62 nm and 626±8.2 nm, with characteristic abundance images for S1, S2 and S3 localizing to RPE LF/MLF consistent with previous reports (11,12).

For fovea, perifovea and mid-periphery—A total of 48 image cubes (4 excitation wavelengths, 12 tissue locations) were decomposed and analyzed. Two foveal samples were inadequate for hyperspectral AF analysis, and one partially recovered only S1 and S2; all of which had large areas of bare BrM. Previously reported spectra S1 and S2 were otherwise observed in all the samples except one donor location which was largely bare BrM (85M Perifovea), where S1 and S3 were recovered, and another where only S2 was recovered (83F Periphery). Interestingly, S3 was recovered from all 3 locations in 88F, the same donor that showed S3 at all 5 drusen positions. However, S3 was otherwise only recovered in Perifovea and Periphery in two donors, 85 M and 81M (4 locations) for 7 total overall. A review of tissues for characteristics that could correlate with the occurrence of the S3 spectrum was inconclusive. SDr was also recovered from one location in which drusen were apparent.

Spectra from the RPE and drusen—Figures 1 and 2 show the "RGB" or panchromatic AF images (at 436 nm excitation) of retina tissues with drusen from an 81-year-old male donor and an 88-year-old female donor, respectively. The spectra shown in both figures are S1, S2 and SDr, while S3 was recovered only from the second donor (Figure 2). The source of S1 is shown in its abundance image, also labeled S1, and is RPE AF that also appears slightly localized to drusen. We attribute this appearance thinned RPE overlying drusen and RPE signal appearing in the combined projection image. The spectrum S2, peaking at about 580 nm, has an abundance quite specific for the RPE. It is interesting that of all donor locations with drusen, only the 5, and all of the five, from donor 88F showed the trimodal spectrum S3 that generally has a primary peak near 630 nm and two secondary peaks at 580 and 650 nm (see Figure 2). We have previously observed the longer wavelength spectrum S3 to be more correlated than S1 and S2 with pigmented structures in the RPE, and therefore have (11,12) posited it to be the AF signal from the organelle melanolipofuscin (MLF). In Figure 2, abundance image S3 co-localizes in part with darker brown spots in the brightfield in a tissue from this donor (presumably containing melanosomes and MLF). The brightfield in Figure 1 by comparison shows evidently less pigment and spectrum S3 was not recovered. However, our study of foveal versus non-foveal tissue for a variance in spectra that may be attributed to greater foveal MLF concentration than extra-foveally was inconclusive.

SDr spectrum comparison between 436 and 450 nm excitation

SDr spectral peaks—Table 1 displays the numbers of SDr peaks that fell between 500 and 530 nm at 436 nm and 450 nm excitations. Almost all fell at 510 or 520 nm for either excitation. The SDr spectrum thus has a consistent characteristic peak at 510 or 520 nm with either excitation 436 and 450 nm.

Spectral shape—Figure 3 shows the SDr spectra that represent drusen and sub-RPE deposits recovered from all 20 samples when the excitations were λ_{ex} 436 and 450 nm. As just noted, the spectra SDr almost all have a peak at 510 or 520 nm. All the spectra of SDr show similar line contours except that from 1 location at 436 nm excitation. The shapes of SDr from the two different excitations are essentially the same. The apparent asymmetry of SDr at 450 nm excitation is due to the cutoff of the long pass emission filter at 495 nm, resulting in rapid drop of intensity below 500 nm, and the intensities of the peaks are slightly different (see NMF spectral output in Figure 1 and Figure 2). Usually, there is a slightly higher SDr peak with λ_{ex} 436 nm excitation compared with 450 nm excitation in our experimental setup with approximately similar radiant energy applied at both excitations. This suggests that the excitation spectrum of SDr is slightly greater at λ_{ex} 436 nm excitation than that at 450 nm excitation.

In a word, the emission spectral signature of drusen and presumably sub-RPE deposits was detected when AMD donor retinal tissues were excited at 436, 450, and 480 nm, peaking at 510 or 520 nm in almost all cases.

Discussion

The potential for hyperspectral AF imaging to be employed clinically for detection and monitoring of drusen and subRPE deposits in AMD has already been demonstrated in

principle *ex vivo* (11). Among remaining challenges, what has not been determined are the *ideal* wavelengths λ_{ex} for excitation of the spectral signature SDr. That question in turn is multi-faceted. Prior work has demonstrated that the recovery of spectral signatures from RPE and related structures in general is strengthened by a multi-excitation wavelength approach, with simultaneous solution of the multiple hyperspectral datasets providing better SNR and smoother solutions (11,12,32,33). A second question, therefore, addressed here, is which *individual* wavelengths are most effective in exciting the signature SDr for inclusion in the multi-excitation approach. Prior work has shown that the combination of λ_{ex} 436 and 480 nm excitation is effective in recovering SDr, and herein we have demonstrated that the intensity of the *individual* signal from λ_{ex} 450 is nearly equivalent to that from 436 nm. 450 nm is a longer wavelength, and hence is less affected by ocular media, and also has less safety concern than 436 nm. Indeed, commercial FDA approved AF cameras operate in this range, e.g., the blue (440–475 nm) excitation in the Eidon Camera (Centervue, Vista, CA). These considerations all suggest that a combination of 450 nm and the classic 480 nm may be the best multi-excitation choice. It is also worth noting that the spectrum SDr was *not* observed in *any* of the 42 tissue locations from 14 normal eyes studied in our previous work (11), suggesting high *specificity* of SDr for AMD eyes.

The study has several limitations. Separation of subRPE deposits into BLinD and BLamD on flat mounts is not possible, and spectrally we only detected one spectrum, SDr, in the 510–520 nm emission range that was attributable to drusen and subRPE deposits collectively. Higher resolution spectral image acquisition in the future might resolve individual spectra, if such exist. Also, our study was not powered to investigate regional differences in RPE AF signal that might be ascribable to recently uncovered detailed mapping of autofluorescent granules (31). Hence our secondary results on foveal *vs.* extrafoveal locations simply recapitulated known RPE spectra.

Conclusions

Hyperspectral AF emission spectra were recovered from 20 AMD tissue samples with drusen at 4 excitations (λ_{ex} 436, 450, 480 and 505 nm) and compared across the emission range 420–720 nm. The known RPE spectra S1, S2 and S3 and the drusen spectrum SDr were consistently recovered, and in particular were recovered from the newly tested λ_{ex} 450 and 505 nm. The pairs of SDr spectra from λ_{ex} 436 and 450 nm exhibited similar shapes and peaks, and SDr spectra from all λ_{ex} were both sensitive and specific to the drusen and apparent sub-RPE deposits, supporting the concept of a single major molecular species of fluorophore in drusen to be determined. These findings may provide vital principles for building a clinical hyperspectral camera with appropriate multi-excitations in the blue range for best detection of sub-RPE deposits consistent with patient safety. Such a clinical camera could detect AMD at its earliest stages for research on its mechanism and to monitor emerging therapies.

Acknowledgments

Funding:

NIH/NEI R01 EY027948 (CC, YT, RTS,TA).

References

1. Hogan MJ. Macular Diseases: Pathogenesis. Electron Microscopy of Bruch's Membrane. Trans Am Acad Ophthalmol Otolaryngol 1965;69:683–90. [PubMed: 14345773]
2. Sarks SH. Ageing and degeneration in the macular region: a clinico-pathological study. Br J Ophthalmol 1976;60:324–41. [PubMed: 952802]
3. Hageman GS, Luthert PJ, Chong NH, et al. An integrated hypothesis that considers drusen as biomarkers of immune-mediated processes at the RPE-Bruch's membrane interface in aging and age-related macular degeneration. Prog Retin Eye Res 2001;20:705–32. [PubMed: 11587915]
4. Khan KN, Mahroo OA, Khan RS, et al. Differentiating drusen: Drusen and drusen-like appearances associated with ageing, age-related macular degeneration, inherited eye disease and other pathological processes. Prog Retin Eye Res 2016;53:70–106. [PubMed: 27173377]
5. Green WR. Histopathology of age-related macular degeneration. Mol Vis 1999;5:27. [PubMed: 10562651]
6. Curcio CA. Soft Drusen in Age-Related Macular Degeneration: Biology and Targeting Via the Oil Spill Strategies. Invest Ophthalmol Vis Sci 2018;59:AMD160–81. [PubMed: 30357336]
7. Ferris FL 3rd, Wilkinson CP, Bird A, et al. Clinical classification of age-related macular degeneration. Ophthalmology 2013;120:844–51. [PubMed: 23332590]
8. Schlanitz FG, Sacu S, Baumann B, et al. Identification of Drusen Characteristics in Age-Related Macular Degeneration by Polarization-Sensitive Optical Coherence Tomography. Am J Ophthalmol 2015;160:335–44.e1. [PubMed: 25982973]
9. Christenbury JG, Folgar FA, O'Connell RV, et al. Progression of intermediate age-related macular degeneration with proliferation and inner retinal migration of hyperreflective foci. Ophthalmology 2013;120:1038–45. [PubMed: 23352193]
10. Zanzottera EC, Messinger JD, Ach T, et al. The Project MACULA Retinal Pigment Epithelium Grading System for Histology and Optical Coherence Tomography in Age-Related Macular Degeneration. Invest Ophthalmol Vis Sci 2015;56:3253–68. [PubMed: 25813989]
11. Tong Y, Ami TB, Hong S, et al. Hyperspectral Autofluorescence Imaging of Drusen and Retinal Pigment Epithelium in Donor Eyes with Age-Related Macular Degeneration. Retina (Philadelphia, Pa) 2016;36:S127–36.
12. Ben Ami T, Tong Y, Bhuiyan A, et al. Spatial and Spectral Characterization of Human Retinal Pigment Epithelium Fluorophore Families by Ex Vivo Hyperspectral Autofluorescence Imaging. Transl Vis Sci Technol 2016;5:5.
13. Curcio CA, Millican CL. Basal linear deposit and large drusen are specific for early age-related maculopathy. Arch Ophthalmol 1999;117:329–39. [PubMed: 10088810]
14. Huang H, Liu L, Ngadi MO. Recent developments in hyperspectral imaging for assessment of food quality and safety. Sensors (Basel) 2014;14:7248–76. [PubMed: 24759119]
15. Xiong Z, Xie A, Sun DW, et al. Applications of hyperspectral imaging in chicken meat safety and quality detection and evaluation: a review. Crit Rev Food Sci Nutr 2015;55:1287–301. [PubMed: 24689678]
16. Edelman GJ, Gaston E, van Leeuwen TG, et al. Hyperspectral imaging for non-contact analysis of forensic traces. Forensic Sci Int 2012;223:28–39. [PubMed: 23088824]
17. Mehta N, Shaik S, Devireddy R, et al. Single-Cell Analysis Using Hyperspectral Imaging Modalities. J Biomech Eng 2018;140:0208021–6.
18. Gowen AA, Feng Y, Gaston E, et al. Recent applications of hyperspectral imaging in microbiology. Talanta 2015;137:43–54. [PubMed: 25770605]
19. Giannoni L, Lange F, Tachtsidis I. Hyperspectral imaging solutions for brain tissue metabolic and hemodynamic monitoring: past, current and future developments. J Opt 2018;20:044009. [PubMed: 29854375]
20. Lambert R. Endoscopy in screening for digestive cancer. World J Gastrointest Endosc 2012;4:518–25. [PubMed: 23293721]
21. Kiyotoki S, Nishikawa J, Okamoto T, et al. New method for detection of gastric cancer by hyperspectral imaging: a pilot study. J Biomed Opt 2013;18:26010. [PubMed: 23389679]

22. Han Z, Zhang A, Wang X, et al. In vivo use of hyperspectral imaging to develop a noncontact endoscopic diagnosis support system for malignant colorectal tumors. J Biomed Opt 2016;21:16001. [PubMed: 26747475]
23. Lu G, Qin X, Wang D, et al. Quantitative Wavelength Analysis and Image Classification for Intraoperative Cancer Diagnosis with Hyperspectral Imaging. Proc SPIE Int Soc Opt Eng 2015;9415:94151B.
24. Yudovsky D, Nouvong A, Pilon L. Hyperspectral imaging in diabetic foot wound care. J Diabetes Sci Technol 2010;4:1099–113. [PubMed: 20920429]
25. Liu C, van Netten JJ, Klein ME, et al. Statistical analysis of spectral data: a methodology for designing an intelligent monitoring system for the diabetic foot. J Biomed Opt 2013;18:126004. [PubMed: 24337494]
26. Milanic M, Paluchowski LA, Randeberg LL. Hyperspectral imaging for detection of arthritis: feasibility and prospects. J Biomed Opt 2015;20:096011. [PubMed: 26359812]
27. Gao L, Smith RT, Tkaczyk TS. Snapshot hyperspectral retinal camera with the image mapping spectrometer (IMS). Biomed Opt Express 2012;3:48–54. [PubMed: 22254167]
28. Baltussen EJM, Kok END, Brouwer de Koning SG, et al. Hyperspectral imaging for tissue classification, a way toward smart laparoscopic colorectal surgery. J Biomed Opt 2019;24:1–9.
29. Panasyuk SV, Yang S, Faller DV, et al. Medical hyperspectral imaging to facilitate residual tumor identification during surgery. Cancer Biol Ther 2007;6:439–46. [PubMed: 17374984]
30. Ach T, Huisingh C, McGwin G Jr, et al. Quantitative autofluorescence and cell density maps of the human retinal pigment epithelium. Invest Ophthalmol Vis Sci 2014;55:4832–41. [PubMed: 25034602]
31. Pollreisz A, Neschi M, Sloan KR, et al. Atlas of Human Retinal Pigment Epithelium Organelles Significant for Clinical Imaging. Invest Ophthalmol Vis Sci 2020;61:13.
32. Smith RT, Post R, Johri A, et al. Simultaneous decomposition of multiple hyperspectral data sets: signal recovery of unknown fluorophores in the retinal pigment epithelium. Biomed Opt Express 2014;5:4171–85. [PubMed: 25574430]
33. Mohammed T, Tong Y, Agee J, et al. Ex Vivo Hyperspectral Autofluorescence Imaging and Localization of Fluorophores in Human Eyes with Age-Related Macular Degeneration. Vision 2018;2:38.

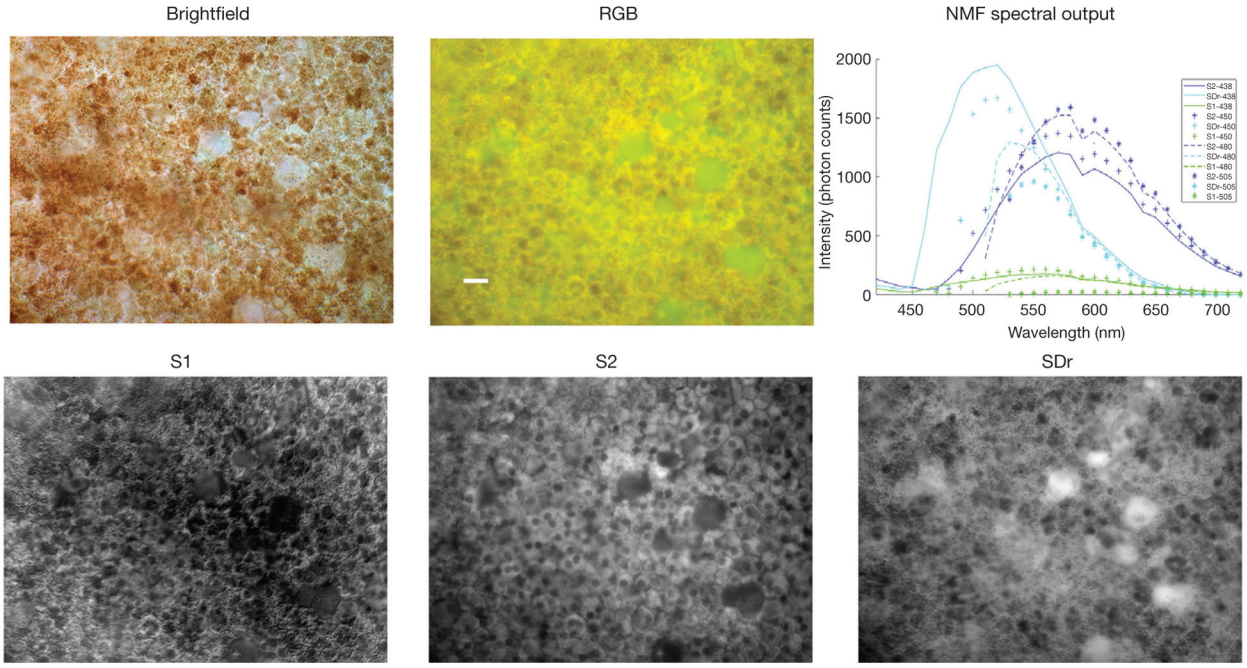

Figure 1.

Hyperspectral AF imaging and analysis of an RPE/BrM flatmount from an 85-year-old male donor with AMD and sub-RPE deposits. RGB, brightfield, abundance images and spectra. Brightfield: Sub-RPE deposits evident as distinct, bright round structures are presumed to be small drusen. RGB: Panchromatic AF image. Presumed drusen are bright green. Other small ill-defined greenish structures may be thin and diffusely distributed subRPE deposits. Scale bar: 50 μm. The corresponding individual recovered spectra are shown in non-negative matrix factorization NMF spectral output: S1 (green lines), S2 (blue lines) and SDr (azure lines). S3 was not recovered from this tissue. Spectra recovered from individual excitations are shown as λ_{ex} 436 nm (solid lines), 450 nm (diamond lines), 480 (dashed lines) and 505 nm (dotted lines). Abundance images for recovered spectra: S1 localized to RPE LF/MLF and slightly to drusen, S2 localized to RPE LF/MLF, and SDr localized to drusen and the other small green structures on the RGB, presumably sub-RPE deposits.

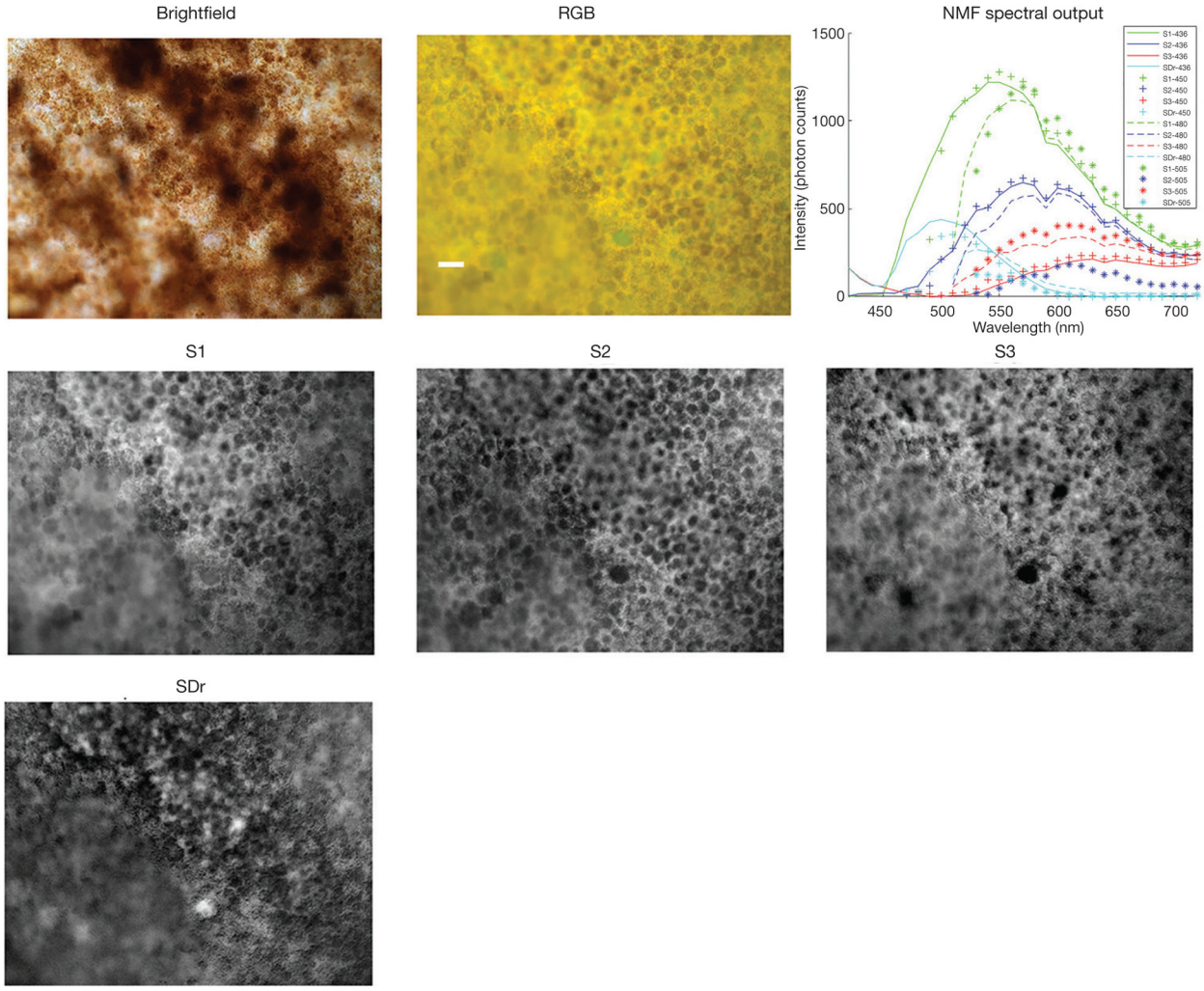

Figure 2.

Hyperspectral AF imaging and analysis of an RPE/BrM flatmount from an 88-year-old female donor with AMD. RGB, brightfield, abundance images and spectra. Brightfield: Distinct, bright round structures are presumed small drusen. RGB: Panchromatic AF image. Drusen are bright green. Other small ill-defined greenish structures may be thin and diffusely distributed subRPE deposits. Scale bar: 50 μm. The corresponding individual recovered spectra are shown in non-negative matrix factorization NMF spectral output: S1 (green lines), S2 (blue lines), S3 (red lines) and SDr (azure lines). Spectra recovered from individual excitations are shown as λ_{ex} 436 nm (solid lines), λ_{ex} 450 nm (diamond lines), λ_{ex} 480 (dashed lines) and λ_{ex} 505 nm (dotted lines). Abundance images for recovered spectra: S1 localized to RPE and slightly to drusen, S2 and S3 localized specifically to RPE LF and MLF, and SDr localized to drusen and presumably sub-RPE deposits.

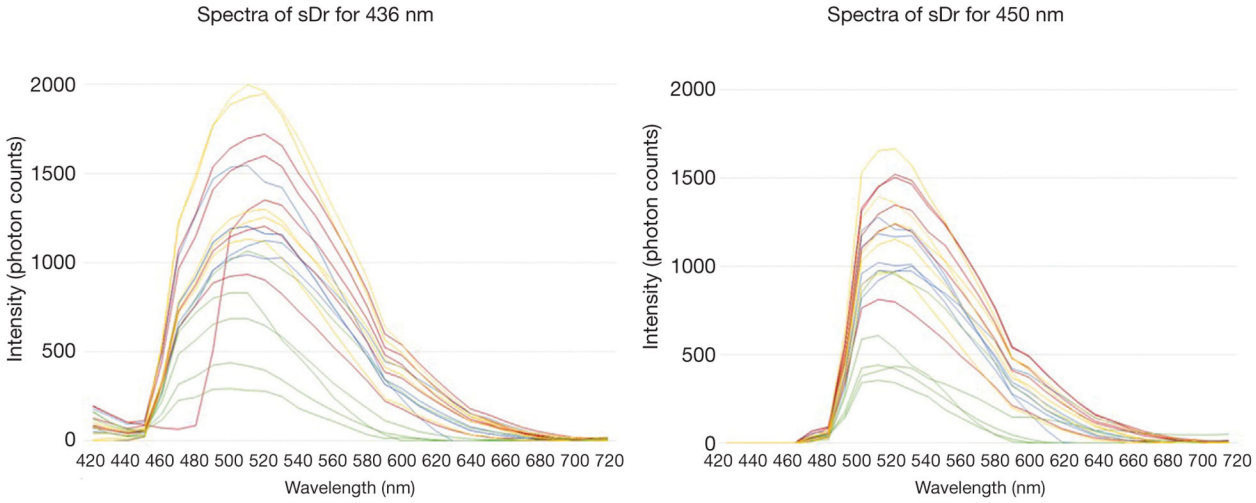

Figure 3.

Spectra SDr of drusen and sub-RPE deposits from 20 AMD samples. Top: λ_{ex} 436 nm. Bottom: λ_{ex} 450 nm. The 5 SDr spectra from each donor (age/gender) are color-coded: 81M (yellow lines), 83F (red lines), 85M (green lines), and 88F (blue lines).

Table 1

Numbers of drusen/subRPE deposit spectra SDr peaking near 510/520 nm from 20 AMD samples at excitation wavelengths λ_{ex} 436 and 450 nm

Excitation wavelength	SDr Peak Locations (nm)			
	500	510	520	530
436 nm	2	10	8	0
450 nm	0	9	10	1

Ann Eye Sci. Author manuscript; available in PMC 2021 March 30.